Journal of Colloid and Interface Science 365 (2012) 254–259

Contents lists available at SciVerse ScienceDirect

Journal of Colloid and Interface Science

www.elsevier.com/locate/jcis

Experimental and theoretical investigations of evaporation of sessile water droplet on hydrophobic surfaces

Ying-Song Yu [a,b], Ziqian Wang [a], Ya-Pu Zhao [a,*]

[a] State Key Laboratory of Nonlinear Mechanics (LNM), Institute of Mechanics, Chinese Academy of Sciences, Beijing 100190, People's Republic of China
[b] Department of Engineering Mechanics, School of Civil Engineering and Architecture, Hubei University of Technology, Wuhan 430068, People's Republic of China

ARTICLE INFO

Article history:
Received 12 June 2011
Accepted 6 September 2011
Available online 10 September 2011

Keywords:
Droplet
Evaporation
Contact angle
Constant contact radius
Hydrophobic surfaces

ABSTRACT

Experiments of sessile water droplet evaporation on both polydimethylsiloxane (PDMS) and Teflon surfaces were conducted. All experiments begin with constant contact area mode (the initial contact angle is greater than 90°), switch to constant contact angle mode and end with mixed mode. Based on the assumptions of spherical droplet and uniform concentration gradient, theoretical analyses for both constant contact area and constant contact angle modes are made and theoretical solutions are derived accordingly, especially a theoretical solution of contact angle is presented first for CCR stage with any value of the initial contact angle. Moreover, comparisons between the theoretical solutions and experimental data of contact angle in CCR stage demonstrate the validity of the theoretical solution and it would help for a better understanding and application of water droplet on solid surfaces, which is quite often encountered in lab-on-a-chip, polymerase chain reaction (PCR) and other micro-fluidics devices.

1. Introduction

In recent decades, water or aqueous solutions with small volume are playing significant roles in micro- and nano-fluidics, lab-on-a-chip, electro-elasto-capillarity (EEC) and so on [1–5]. However, when water is not in equilibrium with its surroundings, it will evaporate [6], leading to some changes, for example, the loss of water or concentration variation, which might affect the performance of these devices and polymerase chain reaction (PCR) amplification efficiency [7]. Therefore, investigations on droplet evaporation are of great concerns in many research fields.

Droplet evaporation is a common and complex diffusion phenomenon driven by the difference of liquid concentration gradient [8], and it is controlled by the physical properties of the liquid itself, such as the molecular weight, density, diffusion coefficient in air, and heat of vaporization [9]. As early as in 1877, Maxwell as a pioneer derived the classic relationship to describe the diffusion-driven evaporation of aerosol droplet [10]. About one century later, Picknett and Bexon [11] first presented two different evaporation modes, namely constant contact area mode (CCR, also called as pinned contact line mode) and constant contact angle mode (CCA, or moving contact line mode). With the assumption of spherical droplet, they gave a theoretical solution of contact radius in CCA stage, and only numerically simulated the CCR-mode. In 1993, based on their own experiments of water droplets evaporating on two different solid surfaces (one is hydrophobic or non-wetting, the other is hydrophilic or wetting) [12,13], Birdi and Vu deduced that evaporation of liquid droplet placed on smooth solid surfaces has two different trends depending on the absolute value of contact angle, i.e., CCR mode for contact angle <90° and CCA mode for contact angle >90° [13]. However, these studies did not work all the way for there is something which should be considered or investigated extensively [14–16]. For example, some experiments on droplet evaporation are reported to follow CCR mode at first when the initial contact angle is larger than 90° [14,17–19]. Actually, the origin of CCR mode is that the three-phase contact line is pinned to the surface. One of the main causes is thought to be contact angle hysteresis [20–22], which mainly arises from molecular interactions between the liquid and solid, or from surface anomalies, such as heterogeneities [20] and surface roughness [23]. Besides, due to the unbalanced force at the three-phase contact line, there will be ridge-like surface deformation induced by sessile liquid droplet [24,25]. The ridge itself is usually small and does not contribute to a significant pinning force, yet, this ridge is associated (also) with a molecular reorientation of the solid molecules at the three phase contact line [2,21]. This molecular reorientation results in a stronger solid–liquid intermolecular interaction, and hence stronger pinning.

Shanahan and Bourgès [26] studied the evolution of contact angles of water on different polymer surfaces in both saturated and nonsaturated atmospheres. Their experiments included three to four stages and evaporation of sessile water droplet on polished epoxy resin first began with CCR mode (the initial contact angle is 61°). One year later, evaporation experiments of water and *n*-decane

* Corresponding author. Fax: +86 10 6256 1284.
E-mail address: yzhao@imech.ac.cn (Y.-P. Zhao).

0021-9797/$ - see front matter © 2011 Elsevier Inc. All rights reserved.
doi:10.1016/j.jcis.2011.09.007

placed on different substrates in nonsaturated environment have been carried out and all experiments began with CCR mode [27]. To describe the influence of evaporation on contact angles, they presented a concept of stagnation layer [26] and gave a model for the analysis of CCR stage [27]. In this model, they assumed that the diffusion of liquid vapor from the drop into the surrounding atmosphere, corresponding to evaporation, is purely radial. In 1995, assuming the concentration gradient to be radially outward and neglecting the edge effect due to the contact line on evaporation of spherical droplet, Rowan et al. [28] deduced a simple relationship of droplet evaporation $dV/dt = -2\pi D(c_\infty - c_0)h/\rho$, where D is the diffusion coefficient of liquid, c_0 and c_∞ are the saturated vapor concentration and the vapor concentration at infinite distance, ρ is the liquid density and h is the droplet height. Based on these assumptions, both CCA [15,29] and CCR (for contact angle <90°) [28] modes were theoretically analyzed. Later, a fitting solution of contact angle was obtained for CCR mode with contact angle between 90° and 180° [30]. Moreover, Butt et al. [31] provided two approximations to study evaporation of sessile liquid drops with constant contact radius for initial contact angle below 90°. Anantharaju et al. [16] experimentally studied evaporation of sessile droplet on smooth and rough surfaces and concluded that the three-phase contact line topology has no effect on the evaporation rate. Besides, Hu and Larson [8] numerically studied CCR mode evaporation and derived an approximate expression for droplet evaporation rate at any contact angle ($0° < \theta < 90°$). The vapor concentration distribution was also simulated, which showed that the concentration gradient was nearly constant. Kim et al. [32] experimentally studied evaporation of water droplets on polymer surfaces and attributed the first and second transitions in the evaporation process to the attainment of the receding contact angle and the Marangoni instability, respectively.

PDMS has many advantages such as good biocompatibility, nontoxic and optically transparent, and easily fabricated [25]. And Teflon is chemically inert and resists both acids and bases and it can be fabricated as hydrophobic surface with very low contact angle hysteresis (<10° for water in air) [33]. Thus PDMS and Teflon are being widely used in micro- and nano-fluidic systems [34,35]. Recently, works on evaporation of water droplet on smooth or patterned PDMS surfaces have been reported [17,18,36]. However, up till now, to the best knowledge of us, no theoretical solution of contact angle has been presented for CCR mode evaporation with any value of the initial contact angle. Therefore, in this paper evaporation experiments of sessile water droplets on PDMS and Teflon surfaces were carried out in still air and room temperature. It is found that all experiments also begin with CCR mode, switch to CCA mode and end with mixed mode. Under the assumptions of spherical droplet and uniform concentration gradient, theoretical analyses for both CCR stage and CCA stage are given and theoretical solutions are derived accordingly, especially a theoretical solution of contact angle in the CCR stage is presented for any value of the initial contact angle. Comparisons between theoretical solution of contact angle and experimental data show that the solution agrees well with experiments. Moreover, the time of CCR stage, variation rate of liquid–vapor interfacial area and the total evaporation time are discussed.

2. Experiments

We prepared both PDMS (Sylgard 184, Dow Corning, USA) and Teflon membranes for studying droplet evaporation. PDMS (mass ratio of base to curing is 10:1) was spin-coated on the surface of clean glass at the rate of about 1000 rpm, then the samples were solidified in 150 °C for 20 min. The thickness of PDMS was about 70 μm [37]. When PDMS was solidified, the 6 wt.% Teflon® 1601 solution (Teflon was dissolved in perfluorinated solvent as supplied by DuPont Polymers, Wilmington DE) was directly spin-coated onto the PDMS at the rate of about 3000 rpm. Then the samples were baked at 110 °C for 10 min, then at 250 °C for 5 min and finally at 340 °C for 5 min [38]. The thickness of Teflon layer was estimated at several to tens micrometers, according to the report by DuPont. In order to reduce the environmental effect on droplet evaporation, a chamber (10.0 cm × 10.0 cm × 3.0 cm) with a small hole at the top side was used. Deionized water droplets with volume V_0 of either 2.0 μl or 4.0 μl were generated by a syringe passing through the hole and deposited in each surface. All experiments were carried out with help of the OCA 20 system (precision: ±0.1°, from Dataphysics, Germany), which was equipped with a high-resolution camera (Fig. 1). The environmental temperature T and relative humidity RH are 23.6 °C and 7.6%, respectively. The diffusion coefficient D is 2.58×10^{-5} m^2/s, and the concentrations of saturated water vapor and vapor far from the droplet are denoted as c_0 (21.30×10^{-3} kg/m^3) and c_∞ ($c_\infty = c_0 \times RH = 1.62 \times 10^{-3}$ kg/m^3), respectively [39]. When droplets were deposited on the surfaces, the OCA 20 system was immediately applied to record the evaporation processes after careful pre-adjustment. Every experiment was repeated at least six times, and evaporation of 2.0 μl water droplet was carried out at least 10 times. Images of the water droplets were extracted with certain time interval from the videos and converted into the dimensionless quantities of contact radius (Fig. 2) and droplet height (Fig. 3), and contact angle (Fig. 4) indicating that all experiments were reproducible. Moreover, Figs. 2–4 showed that droplet evaporation began with CCR mode. With or without a short transition (the contact radius began to decrease, and contact angle might increase), it switched to a second stage, during the stage, contact radius decreased while contact angle had only a small variation (Table 1), therefore, this stage was thought as CCA stage.

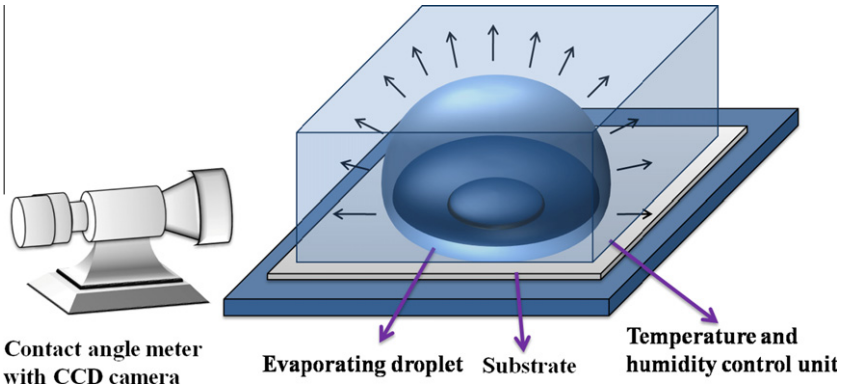

Fig. 1. Experimental schematic of water droplet evaporating on hydrophobic surfaces.

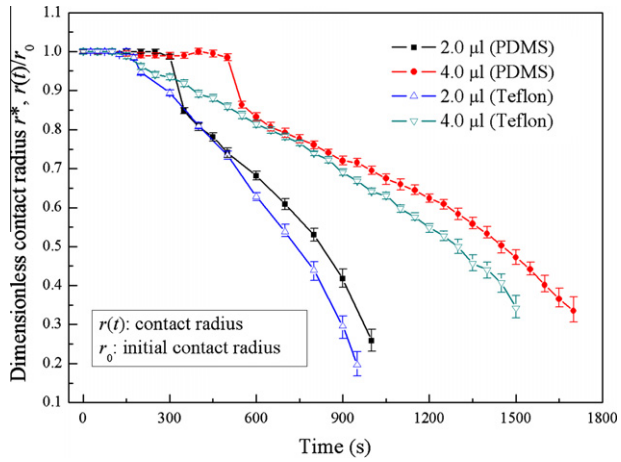

Fig. 2. Dimensionless contact radius of evaporating droplets on hydrophobic surfaces.

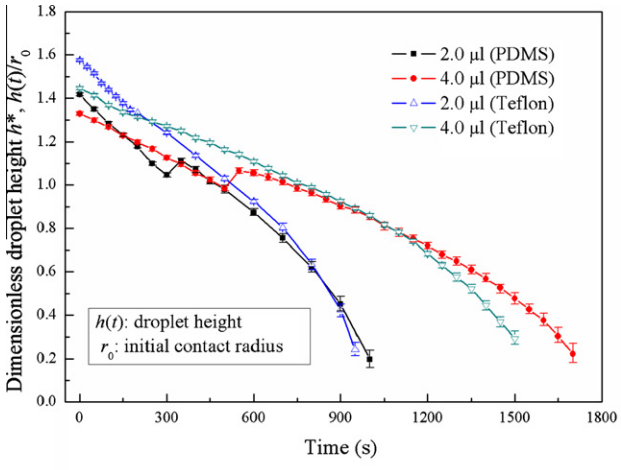

Fig. 3. Dimensionless droplet height of evaporating droplets on hydrophobic surfaces.

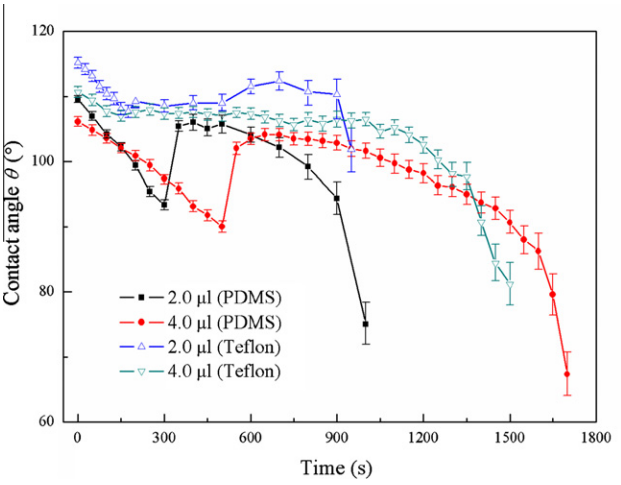

Fig. 4. Contact angle of evaporating droplets on hydrophobic surfaces.

When this stage ended, both contact radius and contact angle decreased during the final stage, which was called as mixed mode. Besides, the total evaporation time, the CCR evaporation time and the CCA evaporation time were measured (Table 1). It was found that for the case of PDMS surface, longer CCR stage corresponded to larger water droplet and a larger variation of contact angle during CCR stage (denoted as $\Delta\theta_{CCR}$), while for the case of Teflon surface, the CCR stage was shorter for larger water droplet and the variation of contact angle was also smaller.

Table 1
Analysis of time of droplet evaporation.

V_0 (μl)	$t_{evaporation}$ (s)	t_{CCR} (s)	t_{CCA} (s)	$\Delta\theta_{CCR}$ (°)	θ_{CCA} (°)
Case A: PDMS surface					
2.0	1100	300	300	9.87	$104.75^{+1.29}_{-2.56}$
4.0	1700	500	500	16.12	$102.79^{+1.34}_{-2.25}$
Case B: Teflon surface					
2.0	1000	175	700	7.49	$110.09^{+2.28}_{-1.55}$
4.0	1600	150	850	3.65	$106.57^{+1.42}_{-2.44}$

3. Theoretical analysis

Under the assumption of spherical droplet, evaporating droplet can be described by using the three parameters, that is, contact radius $r(t)$, droplet height $h(t)$ and contact angle $\theta(t)$ (Fig. 5). And they satisfy the following relationship:

$$h(t) = \frac{1-\cos\theta(t)}{\sin\theta(t)} r(t). \tag{1}$$

The curvature radius of spherical droplet is

$$R(t) = \frac{r(t)}{\sin\theta(t)} = \frac{h(t)}{1-\cos\theta(t)}. \tag{2}$$

Therefore, only two of them can be regarded as independent variables. Accordingly, droplet volume and liquid–vapor interfacial area can be written, respectively, as

$$V = \frac{\pi}{6}h(3r^2+h^2) = \frac{\pi r^3}{3}\frac{f(\theta)}{\sin^3\theta} = \frac{\pi h^3}{3}\frac{f(\theta)}{(1-\cos\theta)^3}, \tag{3}$$

and

$$A_{lv} = \pi(h^2+r^2) = 2\pi r^2\frac{1}{1+\cos\theta} = 2\pi h^2\frac{1}{1-\cos\theta} = 2\pi Rh, \tag{4}$$

where $f(\theta) = 2-\cos\theta(3-\cos^2\theta) = (2+\cos\theta)(1-\cos\theta)^2$.

In this paper, the following dimensionless quantities were used

$$\begin{cases} r^* = \frac{r}{r_0}, \quad h^* = \frac{h}{r_0} \\ h^* = \frac{1-\cos\theta}{\sin\theta} r^* \\ A^*_{lv} = \frac{A_{lv}}{r_0^2} = \pi(h^{*2}+r^{*2}) = 2\pi r^{*2}\frac{1}{1+\cos\theta} = 2\pi h^{*2}\frac{1}{1-\cos\theta}, \\ V^* = \frac{V}{r_0^3} = \frac{\pi}{6}h^*(3r^{*2}+h^{*2}) = \frac{\pi r^{*3}}{3}\frac{f(\theta)}{\sin^3\theta} = \pi h^{*3}\frac{2+\cos\theta}{1-\cos\theta} \end{cases} \tag{5}$$

where r_0 is the initial contact radius. In the experiments by Kim et al. [32], contact radius and droplet height can be determined from the scale of a ruler, which was intended to place the upside of deposited water droplets. However, in our experiments, for the ratio of both contact radius and droplet height with initial contact radius can be determined from fine images. And under the assumption of spherical droplet, the initial contact radius can be obtained with given initial droplet volume. Therefore, evolution of both droplet volume and liquid–vapor interfacial area can also be determined with the help of Eq. (5). Combining Eq. (5) with dimensionless contact radius (Fig. 2) and dimensionless droplet height (Fig. 3), contact angles (Fig. 4) were calculated and all the initial values can be obtained (Table 2). Comparing these with the capillary length of water $l_c = \sqrt{\gamma_{lv}/\rho g} \approx 2.7$ mm, it is found that the characteristic length for

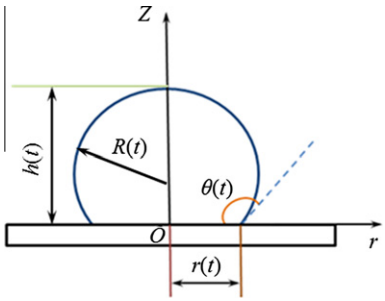

Fig. 5. Side view of spherical droplet.

every case is smaller than capillary length and thus the assumption of spherical droplet is valid.

Usually, droplet evaporation can be simply divided into three stages, namely CCR, CCA and mixed modes. In the CCR stage, the contact area/radius of droplet with solid surface keeps unchanged, that is, the three-phase contact line is pinned, while both the contact radius and droplet height vary with time, thus droplet volume is now a function of contact angle and time; similarly, in the CCA stage, the contact angle is kept unchanged while the contact radius and droplet height decrease, droplet volume is then a function of contact radius (or droplet height) and time. Therefore, taking partial derivative of Eq. (3) with time, the variation rate of droplet volume and liquid–vapor interfacial area can be given, respectively, as

$$\frac{dV}{dt}=\begin{cases}\frac{\pi r_0^3}{(1+\cos\theta)^2}\frac{d\theta}{dt} & (\text{CCR})\\ \pi r^2 f(\theta_1)\frac{dr}{dt} & (\text{CCA})\end{cases}, \tag{6}$$

and

$$\frac{dA_{lv}}{dt}=\begin{cases}-2\pi r_0^2\frac{1}{(1+\cos\theta)^2}\frac{d\cos\theta}{dt} & (\text{CCR})\\ 2\pi\frac{1-\cos\theta_1}{\sin^2\theta_1}\frac{dr^2}{dt} & (\text{CCA})\end{cases}, \tag{7}$$

where θ_1 is the contact angle in the CCA stage.

For evaporation driven by the gradient of vapor concentration, McHale et al. started with Fick's law and assumed that the evaporation rate of spherical droplet for $\theta < 90°$ is given as [28]

$$\frac{dV}{dt}=-\frac{D}{\rho}\int\nabla c\cdot d\mathbf{S}, \tag{8}$$

where ρ is the density of liquid and the integral of the concentration gradient is taken over the total liquid–vapor surface **S** of the spherical cap. Here we suppose that Eq. (8) is also valid for $\theta > 90°$.

For the case of uniform evaporation of a spherical droplet unsupported, the concentration gradient is radially outward and equal to $(c_\infty - c_0)/R$, while for the case of sessile droplet evaporation on solid surface, the concentration gradient is no longer uniform due to the interaction of substrate with liquid droplet, that is, the concentration gradient near the contact line is smaller than that above the surface close to the contact line. However, considering that droplet evaporation is a quasi-steady motion [8] (which could also be found from our experiments), therefore, we neglected the interaction of solid surface and assumed the concentration gradient to be radially outward and equal to $(c_\infty - c_0)/R$ and the assumption is valid for any initial contact angle, then the right-hand side of Eq. (8) can be integrated, and Eq. (8) gives

$$\frac{dV}{dt}=-\lambda h=-\pi\lambda r\frac{1-\cos\theta}{\sin\theta}=\begin{cases}-\pi\lambda r_0\frac{1-\cos\theta}{\sin\theta} & (\text{CCR})\\ -\pi\lambda r\frac{1-\cos\theta_1}{\sin\theta_1} & (\text{CCA})\end{cases}, \tag{9}$$

where $\lambda=\frac{2D(c_0-c_\infty)}{\rho}$, which was uniquely determined by the intrinsic properties of the liquid.

Combining Eq. (9) with Eq. (6), we can get the following differential equations with either contact angle or contact radius as

$$\frac{r_0^2}{(1+\cos\theta)^2}\frac{d\theta}{dt}=-\lambda\frac{1-\cos\theta}{\sin\theta}\ (\text{CCR}), \tag{10}$$

and

$$rf(\theta_1)\frac{dr}{dt}=-\lambda\frac{1-\cos\theta_1}{\sin\theta_1}\ (\text{CCA}), \tag{11}$$

respectively.

For the case of CCA stage, by solving the partial differential equation, Eq. (11), theoretical solution of contact radius can be given as

$$r^2-r_1^2=-2\lambda\frac{\sin^2\theta_1}{(1-\cos\theta_1)(2+\cos\theta_1)}t. \tag{12}$$

where r_1 is the initial contact radius in the stage. Obviously, Eq. (12) is similar to that by Erbil et al. [15].

For the case of CCR stage, McHale et al. gave a theoretical solution for contact angle <90° [28] and a fitting solution for contact angle >90° [30]. For we supposed that the concentration gradient is uniform no matter what the contact angle is, dynamic contact angle during CCR stage can be obtained by solving the partial differential equation, Eq. (10), and given as

$$F(\theta)-F(\theta_0)=-2\lambda t/r_0^2, \tag{13}$$

where $F(\theta)=\ln[\tan(\theta/2)]+1/(1+\cos\theta)$. Though it is difficult to get an explicit expression of contact angle, the contact angle can be easily determined with the help of mathematical software such as Mathematica. Moreover, it should be noted that all the above analyses are supposed to be valid for both hydrophobic and hydrophilic surfaces.

4. Comparison and discussion

As we know, CCA mode evaporation has been theoretically analyzed by Picknett and Bexon [11], and McHale et al. [15,29], and the solutions agree well with experiments. Therefore, the first thing of interest is to demonstrate the validity of theoretical analysis of CCR stage, namely Eq. (13) for dynamic contact angle. All parameters necessary for the analysis are listed in Table 2. Substituting the corresponding parameters into Eq. (13), theoretical solution of dynamic contact angle during CCR stage for every experiment is obtained and then compared with the experimental data (Fig. 6).

Table 2
Parameters for analysis of CCR stage.

$D = 2.58\times10^{-5}$ m^2/s, $c_0 = 21.30\times10^{-3}$ kg/m^3, $c_\infty = 1.62\times10^{-3}$ kg/m^3, $\lambda = 1.016\times10^{-9}$ m^2/s

Surface	V_0 (μl)	h_0/r_0	θ_0 (°)	r_0 (mm)	λ_1 (10^{-3}/s)
PDMS	2.0	1.417	109.58	0.813	1.537
	4.0	1.330	106.12	1.064	0.897
Teflon	2.0	1.576	115.20	0.762	1.749
	4.0	1.446	110.67	1.012	0.992

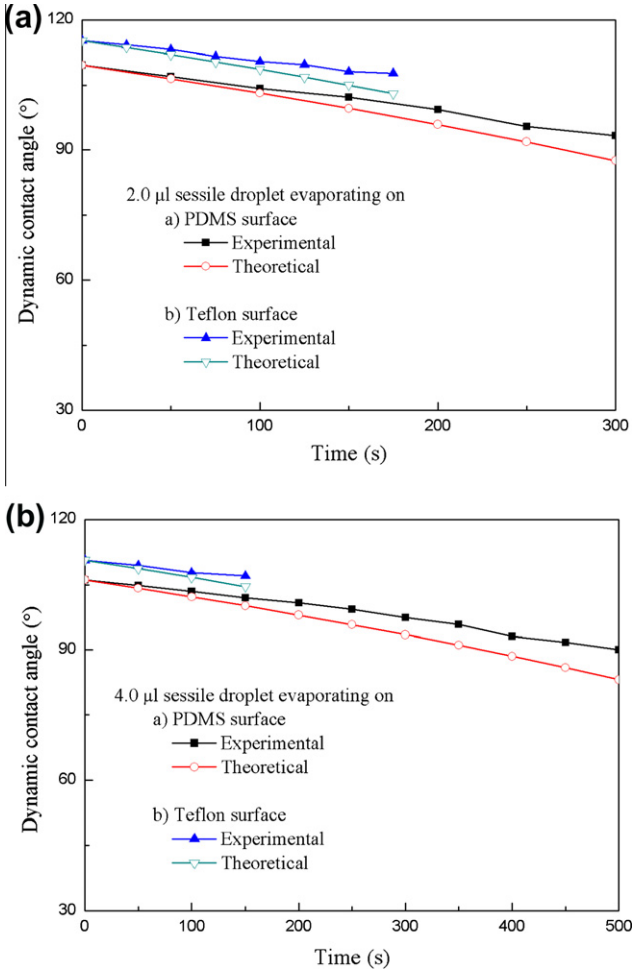

Fig. 6. Comparisons of contact angle of (a) 2.0 μl and (b) 4.0 μl sessile water droplets deposited on both PDMS and Teflon surfaces.

The relative errors are all small at the beginning and increases with time, the largest relative errors are all smaller than 7.0%.

To further check the validity of our solution, we have found one article [32], in which evaporation of sessile droplet with different initial volume on polymethylmethacrylate (PMMA) and poly(α-methyl styrene) (PAMS) surfaces were reported. The temperature and relative humidity were approximately constant at 25–26 °C and 53 ± 1%, respectively. Then diffusion coefficient and the saturated concentration of water vapor at 25 °C are approximately 2.61×10^{-5} m^2/s and 21.3×10^{-3} kg/m^3 [39], respectively. The experimental data of contact angle were determined by using Eq. (1) when contact radius and droplet height were measured. The theoretical ones are obtained by substituting the corresponding parameters (Table 3) into Eq. (13), and were compared with experiments (Fig. 7). The relative errors are less than 4.0%. In a word, the theoretical analysis of CCR stage is valid no matter whether the initial contact angle is larger or less than 90°.

Though the difference of concentration gradient along the liquid–vapor interface is ignored, the theoretical solution agrees well with

Table 3
Parameters for analysis of CCR stage (data from [32]).

V_0 (μl)	Surface	r_0^* (mm)	h_0^* (mm)	V_0^* (μl)	V_{err} (%)
2.19	PMMS	1.202	0.823	2.16	−1.37
2.14	PAMS	1.012	1.039	2.26	5.60

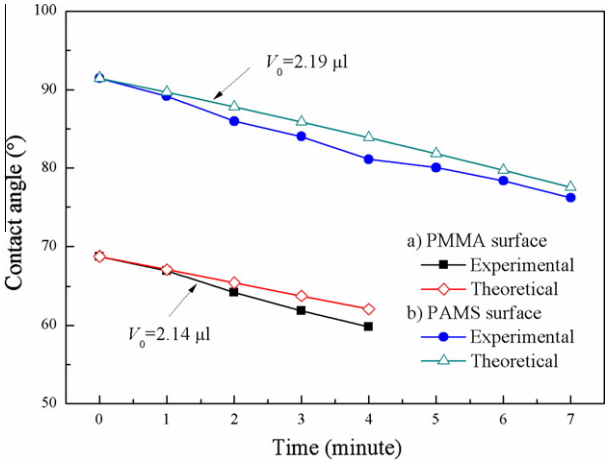

Fig. 7. Comparisons of contact angle: (a) sessile water droplet with initial volume of 2.19 μl evaporating on PMMA surface; (b) sessile water droplet with initial volume of 2.14 μl evaporating on PAMS surface.

experiments by comparisons. However, it should be noted that more experiments of sessile droplet evaporation on different surfaces, especially with either higher or lower contact angle, are necessary to check the validity of our theoretical analysis.

The second thing of interest is the time of CCR stage, which can be estimated from Eq. (13) and expressed as

$$t = \frac{\rho r_0^2}{4D(c_0 - c_\infty)}[F(\theta_0) - F(\theta)] = \frac{\rho r_0^2}{4D(c_0 - c_\infty)}[F(\theta_0) - F(\theta_0 - \Delta\theta)], \quad (14)$$

where $\Delta\theta$ is the difference between initial and dynamic contact angles. From Eq. (14), the total time of CCR stage is found on the order of $\frac{\rho r_0^2}{4D(c_0 - c_\infty)}$, which means that the total CCR time depends sharply on the square of contact radius, and the proportional ratio is the dimensionless parameter $F(\theta_0) - F(\theta_0 - \Delta\theta)$, which depends on both the initial contact angle and contact angle variation during this stage (Fig. 8). Combining this figure with Eq. (14), it can be found that if the environmental conditions and initial contact radius were unchanged, (i) increment in variation of contact angle corresponds to increment in total CCR time; (ii) if the variation of contact angle is also fixed, the total CCR time are almost unchanged for the case of

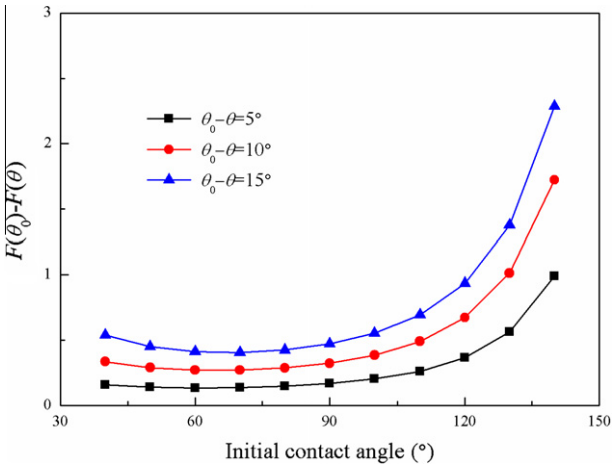

Fig. 8. Dependence of dimensionless function $F(\theta_0) - F(\theta)$ on initial contact angle with fixed contact angle variation.

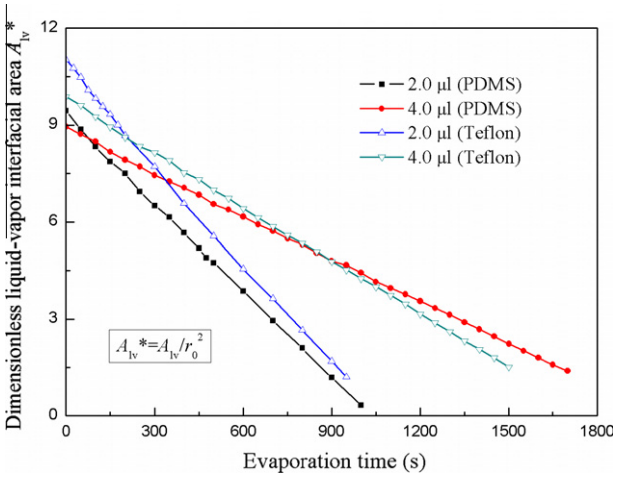

Fig. 9. Dimensionless liquid–vapor interfacial area during evaporation process.

initial contact angle <90°, while it will increase monotonically with the increase of initial contact angle, which is larger than 90°.

The third thing of interest is variation rate of liquid–vapor interfacial area. Substituting the theoretical solutions for both CCR and CCA stages into the expression of variation rate of dynamic liquid–vapor area, Eq. (7), we can get

$$\frac{dA_{lv}}{dt}=\begin{cases}-2\pi\lambda(1-\cos\theta), & (\text{CCR})\\ -\frac{4\pi\lambda}{2+\cos\theta_1}, & (\text{CCA})\end{cases} \tag{15}$$

From Eq. (15), it was found that variation rates of dynamic liquid–vapor area in the two stages are on the order of λ unless the contact angles are approaching to 180°. As shown in Table 2, the parameter λ is about 10^{-9} m^2/s, which means the variation rates during the two stages can be regarded as equal. Substituting the experimental data of dimensionless contact radius and droplet height into Eq. (5), the dimensionless liquid–vapor interfacial area was found to decrease linearly with time (Fig. 9) (this conclusion is also found in literature such as [12,32]). If this is adopted for mixed mode, then the evaporation process follows the relationship, and the total evaporation time is estimated as

$$t_{\text{evaporation}}\sim\frac{A_{lv}^0}{\lambda}\sim\frac{V_0^{2/3}}{\lambda}. \tag{16}$$

5. Conclusions

Experiments of sessile water droplet evaporating on both PDMS and Teflon surfaces have been conducted and it is found that all experiments begin with CCR mode, switch to CCA mode after a short transition and end with mixed mode (Fig. 3). Based on the assumption of spherical droplet and uniform concentration gradient, uniform concentration gradient across the liquid–vapor interface, both CCR and CCA stages are theoretically analyzed and theoretical solutions are derived accordingly (Eqs. (12) and (13)). Comparisons between the theoretical solution and experimental data of contact angle during CCR stage show that the theoretical solution agrees well with experimental data. The total time of CCR stage was found to be sharply dependent on contact radius, and it increase monotonically with the increase of contact angle variation. Moreover, if other parameters are kept unchanged, it is almost the same for initial contact angle <90°, otherwise, increasing initial contact angle corresponds to increment in total CCR time (Fig. 9). Furthermore, the variation rate of liquid–vapor interfacial area is analyzed, which demonstrates that the rate is a function of dynamic contact angle during CCR stage and is constant during CCA stage, and the rates are on the order of $D(c_0-c_\infty)/\rho$, which could be used to predict the total evaporation time.

Acknowledgments

This work was jointly supported by the National Natural Science Foundation of China (NSFC, Grant Nos. 11002051 and 11072244) and the National Basic Research Program of China (973 Program, Grant No. 2007CB310500).

References

[1] A.J. deMello, Nature 422 (2003) 28.
[2] R. Tadmor, P. Bahadur, A. Leh, H.E. Nguessan, R. Jaini, L. Dang, Phys. Rev. Lett. 103 (2009) 266101.
[3] V. Dugas, J. Broutin, E. Souteyrand, Langmuir 21 (2005) 9130.
[4] Q.Z. Yuan, Y.P. Zhao, Phys. Rev. Lett. 104 (2010) 246101.
[5] M. Marinescu, M. Urbakh, T. Barnea, A.R. Kucernak, A.A. Kornyshev, J. Phys. Chem. C 114 (2010) 22558.
[6] M.E.R. Shanahan, Langmuir 18 (2002) 7763.
[7] R.S. Cha, W.G. Thilly, Genome Res. 3 (1993) S18.
[8] H. Hu, R.G. Larson, J. Phys. Chem. B 106 (2002) 1334.
[9] X.H. Fang, B.Q. Li, E. Petersen, Y. Ji, J.C. Sokolov, M.H. Rafailovich, J. Phys. Chem. B 109 (2005) 20554.
[10] J.C. Maxwell, Diffusion-Collected Scientific Papers, Encyclopedia Britannica, Cambridge, 1877.
[11] R.G. Picknett, R. Bexon, J. Colloid Interface Sci. 61 (1977) 336.
[12] K.S. Birdi, D.T. Vu, J. Phys. Chem. 93 (1989) 3702.
[13] K.S. Birdi, D.T. Vu, J. Adhes. Sci. Technol. 7 (1993) 485.
[14] H.Z. Yu, D.M. Soolaman, A.W. Rowe, J.T. Banks, ChemPhysChem 5 (2004) 1035.
[15] H.Y. Erbil, G. McHale, M.I. Newton, Langmuir 18 (2002) 2636.
[16] N. Anantharaju, M. Panchagnula, S. Neti, J. Colloid Interface Sci. 337 (2009) 176.
[17] D.H. Shin, S.H. Lee, C.K. Choi, S. Retterer, J. Micromech. Microeng. 20 (2010) 055021.
[18] X.H. Fang, M. Pimentel, J. Sokolov, M. Rafailovich, Langmuir 26 (2010) 7682.
[19] S.A. Kulinich, M. Farzaneh, Appl. Surf. Sci. 255 (2009) 4056.
[20] C.W. Extrand, Langmuir 19 (2003) 3793.
[21] R. Tadmor, Soft Matter 7 (2011) 1577.
[22] W.Y.L. Ling, T.W. Ng, A. Neild, Q. Zheng, J. Colloid Interface Sci. 354 (2011) 832.
[23] J.G. Fan, Y.P. Zhao, Langmuir 26 (2010) 8245.
[24] R. Pericet-Camara, G.K. Auernhammer, K. Koynov, S. Lorenzoni, R. Raiteri, E. Bonaccurso, Soft Matter 5 (2009) 3611.
[25] Y.S. Yu, Y.P. Zhao, J. Colloid Interface Sci. 339 (2009) 489.
[26] M.E.R. Shanahan, C. Bourgès, Int. J. Adhes. Adhes. 14 (1994) 201.
[27] C. Bourgès-Monnier, M.E.R. Shanahan, Langmuir 11 (1995) 2820.
[28] S.M. Rowan, M.I. Newton, G. McHale, J. Phys. Chem. 99 (1995) 13268.
[29] G. McHale, S.M. Rowan, M.I. Newton, M.K. Banerjee, J. Phys. Chem. B 102 (1998) 1964.
[30] G. McHale, S. Aqil, N.J. Shirtcliffe, M.I. Newton, H.Y. Erbil, Langmuir 21 (2005) 11053.
[31] F. Schönfeld, K.H. Graf, S. Hardt, H.J. Butt, Int. J. Heat Mass Transfer 51 (2008) 3696.
[32] J.H. Kim, S.I. Ahn, J.H. Kim, W.C. Zin, Langmuir 23 (2007) 6163.
[33] F. Mugele, J.C. Baret, J. Phys. Condens. Matter 17 (2005) R705.
[34] T.G. Henares, M. Takaishi, N. Yoshida, S. Terabe, F. Mizutani, R. Sekizawa, H. Hisamoto, Anal. Chem. 79 (2007) 908.
[35] H. Moon, S.K. Cho, R.L. Garrel, C.J. Kim, J. Appl. Phys. 92 (2002) 4080.
[36] C. Luo, M.M. Xiang, X.C. Liu, H. Wang, Microfluid Nanofluid 10 (2011) 831.
[37] W. Dai, Y.P. Zhao, Int. J. Nonlinear Sci. Numer. Simul. 8 (2007) 519.
[38] S.A. Makohliso, L. Giovangrandi, D. Léonard, H.J. Mathieu, M. Ilegems, P. Aebischer, Biosens. Bioelectron. 13 (1998) 1227.
[39] R.C. Weast, M.J. Astle, CRC Handbook of Chemistry and Physics, 62nd ed., CRC Press, Boca Raton, FL, 1981–1982.